CrystEngComm

PAPER

View Article Online
View Journal | View Issue

Cite this: *CrystEngComm*, 2015, **17**, 2013

An *in situ* EDXRD kinetic and mechanistic study of the hydrothermal crystallization of TiO_2 nanoparticles from nitric acid peptized sol–gel

Mohammad Rehan,[ab] Girish M. Kale[c] and Xiaojun Lai*[a]

Received 14th November 2014,
Accepted 13th January 2015

DOI: 10.1039/c4ce02270j

www.rsc.org/crystengcomm

In situ energy dispersive X-ray diffraction (EDXRD) has been used to monitor the crystallization of TiO_2 nanoparticles from hydrothermal reactions of nitric acid (HNO_3) peptized sol–gels at 210, 230, 250 and 270 °C. The EDXRD peaks revealed the formation of pure rutile phase TiO_2 particles from all the hydrothermal reactions studied. The reaction kinetic data have been determined by monitoring changes in the integrated peak areas of the highest intensity diffraction peak (110). A kinetic and mechanistic analysis of the hydrothermal synthesis of TiO_2 nanoparticles has been proposed based on the Avrami–Erofe'ev kinetic model. The Avrami exponent values obtained were within the range of around 0.5–1 for all the reactions studied, indicating that the hydrothermal crystallization of TiO_2 nanoparticles involves a diffusion-controlled process mechanism. The as-synthesized TiO_2 nanoparticles have been further characterized by powder X-ray diffraction (XRD) and transmission electron microscopy (TEM). The XRD data are in good agreement with the EDXRD results and confirm the formation of pure rutile phase TiO_2 particles. The TEM results showed that the TiO_2 particles produced are below 100 nm in size and exhibit bi-modal size and morphology distribution.

Introduction

TiO_2 has attracted wide scientific and technological interest as a result of its applications in photocatalysis, optical devices, gas sensors, solar cells, and antibacterial activity, in the recent past.[1–6] The possibilities of new and enhanced current applications further increase when the material is made in the nanometer size range due to its unique physical, chemical, mechanical and optical properties. This has led to many breakthroughs in the preparation, modification and applications of TiO_2 nanomaterials to date.[7–14]

The hydrothermal process, in which chemical reactions occur in aqueous or organo-aqueous media, under the simultaneous application of heat and pressure, has been widely used to produce TiO_2 nanoparticles.[15–23] This process has many advantages such as it uses relatively low reaction temperatures to obtain particles with narrow particle size distribution, reduces agglomeration and has good phase homogeneity and controlled particle morphology. Despite all the advantages, one major challenge of the hydrothermal process is the difficulty of direct observation of the crystals as they grow due to the black box nature of the process.[24] The use of pressure vessels along with a large number of reaction variables present, including reaction temperature, time, solvent and reactant concentrations and percent fill, contributes to the lack of control in these reactions.[25]

In order to achieve good control of the hydrothermal synthesis of nanoparticles with precisely tailored properties, a better understanding of the reaction kinetics and growth mechanism is essential. An *in situ* monitoring of hydrothermal reactions using synchrotron radiation EDXRD has been used to obtain information to probe the reaction kinetics and mechanisms.[26,27] The high photon energy white X-ray beam of synchrotron radiation has the ability to penetrate into the stainless steel pressure vessel, providing time-resolved diffraction patterns of crystalline materials on an energy scale. This allows an entire diffraction pattern of the contents of the reaction vessel to be collected *in situ* in a short time span (*e.g.* 60 s).[28] The non-invasive EDXRD technique has been developed as a powerful tool at Synchrotron Radiation Source (SRS) station 16.4 at Daresbury Laboratory with various applications of *in situ* process observations such as process tomography, hydrothermal crystallization microporous materials synthesis, chemical reactions, ambient pressure crystallization, and crystal phase transformation reactions.[29–40] In

[a] *Institute of Particle Science and Engineering (IPSE), School of Chemical and Process Engineering, University of Leeds, Leeds LS2 9JT, UK. E-mail: x.lai@leeds.ac.uk; Fax: +44 (0)113 343 2405; Tel: +44 (0)113 343 2439*
[b] *Center of Excellence in Environmental Studies (CEES), King Abdulaziz University (KAU), Jeddah, Saudi Arabia. E-mail: dr.mohammad_rehan@yahoo.co.uk; Tel: +966 583047435*
[c] *Institute for Materials Research (IMR), School of Chemical and Process Engineering, University of Leeds, Leeds LS2 9JT, UK. E-mail: g.m.kale@leeds.ac.uk; Fax: +44 (0)3 343 2384; Tel: +44 (0)113 343 2805*

addition to these, some other applications of *in situ* techniques to study the sol–gel synthesis and crystallization reactions have also been reported recently.[41–49]

In this paper, we present the use of *in situ* EDXRD at station 16.4 of Daresbury Laboratory SRS to study the hydrothermal synthesis of TiO_2 nanoparticles. The nanoparticles have been synthesized by hydrothermal reactions of HNO_3 peptized sol–gels at 210, 230, 250 and 270 °C. The as-synthesized nanoparticles have also been characterized by XRD and TEM analyses. A kinetic and mechanistic analysis of the hydrothermal synthesis of TiO_2 nanoparticles based on the Avrami–Erofe'ev kinetic model has also been reported.

Experimental

Titanium butoxide ($Ti(OBu)_4$) used as a Ti precursor, 2-propanol ($(CH_3)_2CHOH$) used as solvent and nitric acid (HNO_3, 70%) used as a peptizing agent were all obtained from Sigma-Aldrich, UK and used without further purification. A 0.5 M solution of titanium butoxide in 2-propanol was prepared and then added dropwise to distilled water at a 1 : 4 volume ratio with continuous stirring for about 1 hour. The obtained suspension was filtered to collect the white precipitate of hydrolysed TiO_2. The HNO_3 peptized sol–gel was then prepared by stirring a mixture of 31 g of the TiO_2 precipitate, 2.7 ml of HNO_3 (70%) and 90 g of distilled water for about 45 min. This produced a clear pale yellow coloured sol–gel. These sol–gels were then treated hydrothermally at different temperatures to produce TiO_2 nanoparticles.

The hydrothermal synthesis of TiO_2 nanoparticles from HNO_3 peptized sol–gels was monitored *in situ* using EDXRD in Station 16.4 of the SRS at Daresbury Laboratory, UK. The details of the station and the experimental setup can be found in our previous work.[50] In a typical hydrothermal process, 20 ml of the HNO_3 peptized sol–gel was placed in a 30 ml PTFE lined pressure vessel and heated to desired temperature. A special inconel thinner-walled pressure vessel was used to minimize the absorption of X-rays. The hydrothermal reaction mixture was stirred continuously using a PTFE coated magnetic stirrer placed in the vessel to ensure that the particles produced remained in the pathway of the beam throughout the reaction and did not settle down. Four hydrothermal reactions were studied at four different temperatures of 210, 230, 250 and 270 °C with a heating rate of ~10 °C min^{-1}.

During each hydrothermal reaction, the X-ray diffraction patterns were simultaneously collected every 60 s on an energy scale using three-element solid-state detectors; top, middle and bottom, fixed at 2θ angles of 7.375°, 4.51° and 1.61°, respectively. The three-element solid state detector setup used in this work is described elsewhere.[51,52] The raw data recorded by Pincer software during the course of hydrothermal reactions were in channel numbers, which were converted to the energy scale (keV) using a program called DL Convertor. The patterns on the energy scale were then converted to the *d*-spacing scale (Å) using the modified form of Bragg's law:

$$E = 6.199/(d \sin\theta) \quad (1)$$

All hydrothermal reaction products were further characterized using powder XRD and TEM. The equipment, sample preparation and conditions used for this characterization were exactly the same as those described in our previous work.[50]

Results and discussion

The *in situ* EDXRD spectra collected during the hydrothermal synthesis of TiO_2 nanoparticles from HNO_3 peptized sol–gels treated at 210, 230, 250 and 270 °C are shown in Fig. 1(a)–(d) respectively. As the hydrothermal reactions proceeded, the pressure of each vessel started to build up after 30 to 40 min and then stabilized after the attainment of the set temperature. The maximum pressure values observed were around 20, 34, 40 and 42 bar for reactions at 210, 230, 250 and 270 °C, respectively.

In all experiments, the first few EDXRD spectra only showed a broad hump between 1.5 to 4.5 Å *d*-spacing with no Bragg peaks. This hump is produced by the diffuse scattering of the complex structured gel in the reaction vessel and the spectral intensity profile of the white beam.[29] During the hydrothermal reaction of HNO_3 peptized sol–gel at 210 °C, the first diffraction peak emerged with a *d*-spacing value of 3.26 Å after an induction time of 34 min, corresponding to the (110) plane of the rutile crystal structure (Fig. 1a). As the reaction proceeded further, the intensity of this peak increased gradually until around 90 min and then almost stabilized for the rest of the reaction time. Another peak with lower intensity was noticed shortly after the first one with a *d*-spacing value of 2.50 Å, corresponding to the (101) plane of the rutile crystal structure. The intensity of this second peak (101) remained lower than the first one (110), throughout the whole reaction time.

The hydrothermal processes heated up to 230, 250 and 270 °C also showed very similar peak emergence and development akin to that observed at 210 °C. The two same Bragg peaks of *d*-spacings 3.26 and 2.50 Å, corresponding to rutile (110) and (101) diffraction planes, respectively, were observed. However the induction times, 33, 31 and 30 min for the processes at 230, 250 and 270 °C, respectively, were slightly lower than that for the process at 210 °C. Furthermore, the overall peak intensities for the processes at higher temperatures are greater than the process at the lower temperature, which can be attributed to the larger number and size of particles produced at higher process temperature.

There were two small diffraction peaks noticed at *d*-spacings 2.10 and 2.19 Å for the whole reaction period of 250 and 270 °C (Fig. 1(c) and (d)), which do not match with any of the rutile diffraction planes in the reference patterns. These peaks are probably arising from the fluorescence

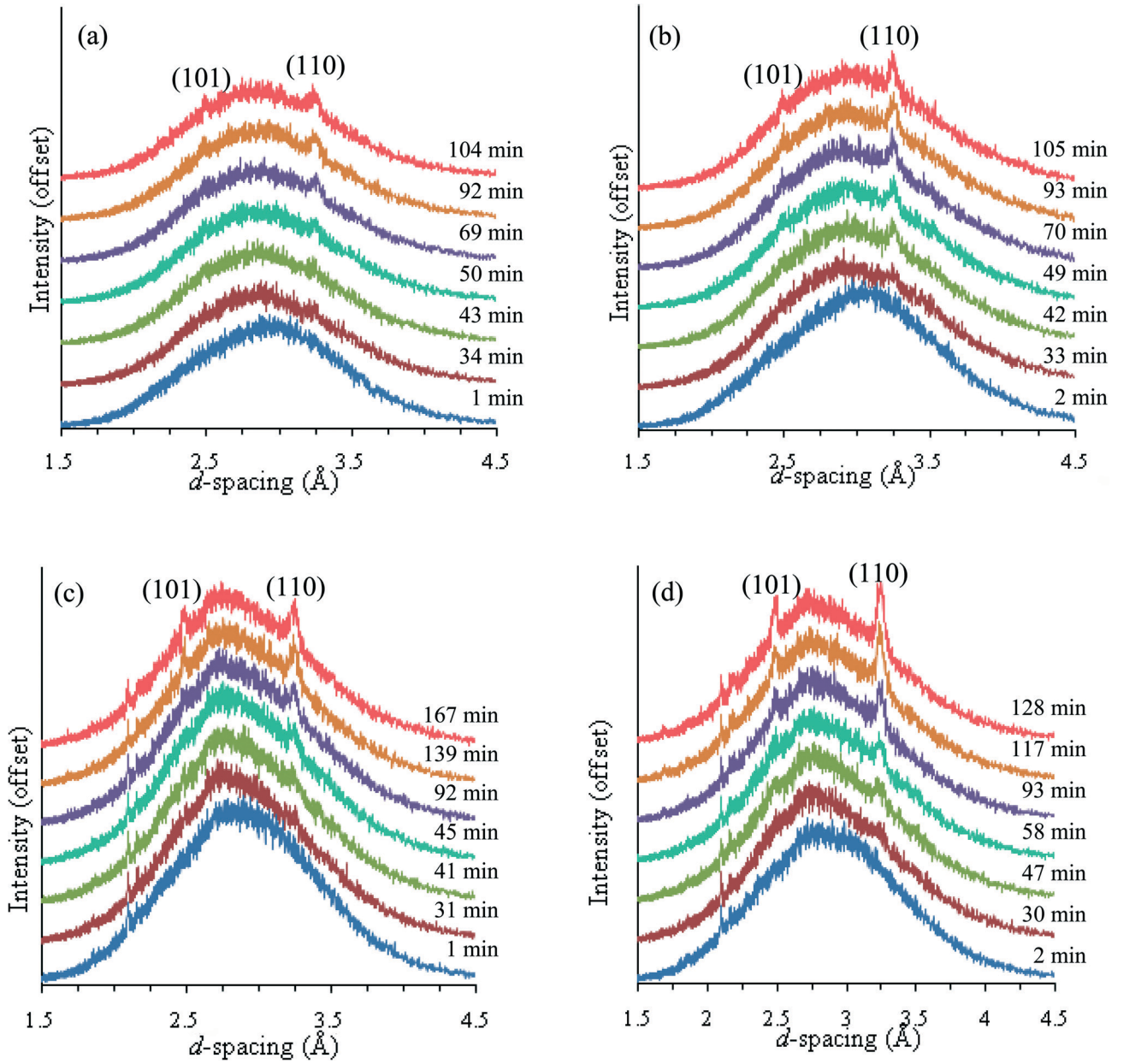

Fig. 1 *In situ* EDXRD data collected during the hydrothermal synthesis of TiO_2 nanoparticles from HNO_3 peptized sol–gels at (a) 210 °C, (b) 230 °C, (c) 250 °C and (d) 270 °C. Modified versions of our previously published EDXRD graphs.[50]

or escape peaks associated with synchrotron beam conditions on the day of the experiment. The data shown in Fig. 1(a) and (b) were obtained on a different experimental day and hence these two additional peaks are not present. The EDXRD patterns show that the rutile phase TiO_2 particles are directly produced from the sol–gel complex structure upon hydrothermal treatment without formation of any crystalline intermediate phase.

The extent of reaction (α) has been measured using the integrated areas of the highest intensity peak (110) and plotted against the reaction time for each hydrothermal process studied (Fig. 2a–d). The peak area is integrated using the Gaussian function by an in-house developed program (XRD Peak Area Analyser). These values can be converted to extent of reaction (α), scaled from zero to one, using the relationship:

$$\alpha(t) = I_{hkl}(t)/I_{hkl}(\max) \quad (2)$$

where $I_{hkl}(t)$ is the area of a given peak at time t and $I_{hkl}(\max)$ is the maximum area of this peak at the point of termination of the reaction. The extent of reaction curves (Fig. 2a–d) roughly follow the sigmoidal profile, where the crystallization process shows slow rates at the beginning and the end of the reaction but fast in between. The slow rate at the beginning is due to the induction period, which represents the time

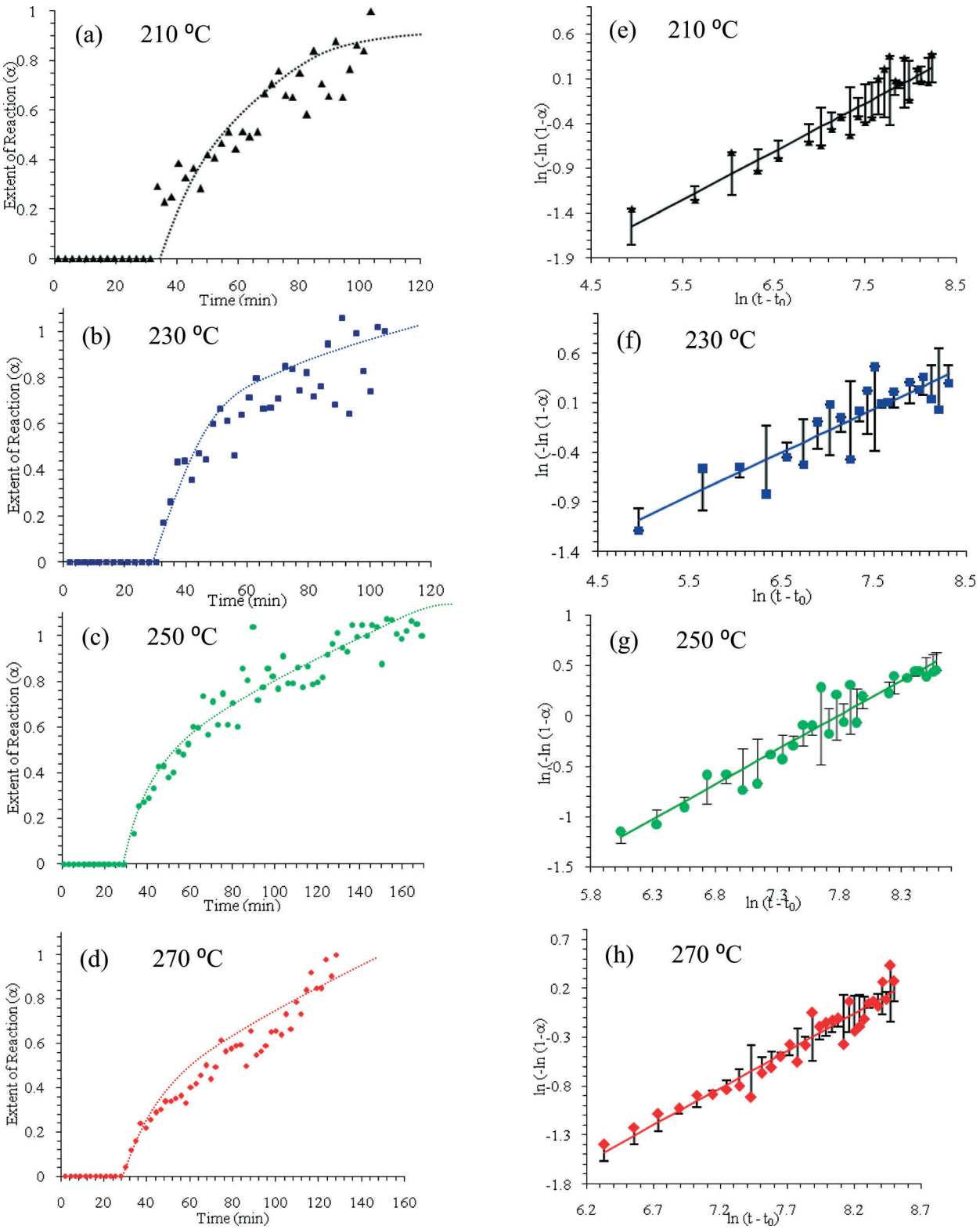

Fig. 2 Extent of reaction against time for the (110) peak of TiO_2 particles produced by *in situ* hydrothermal processes at 210, 230, 250 and 270 °C (a–d) and their corresponding Sharp and Hancock plots showing the kinetic data (e–h), respectively.

taken to produce enough number of nuclei that could potentially be detected by EDXRD. The particles rapidly grow from these nuclei during the intermediate stage. The slow rate in the final stage indicates that the reaction is near to completion after consumption of all the available nuclei. A similar trend is observed in Fig. 2(a–d), further indicating that each hydrothermal process investigated in this study follows an identical reaction mechanism. The dotted lines on

these graphs are constructed manually for easy graph reading and have no physical significance.

The quantitative kinetic analysis of the hydrothermal synthesis of TiO_2 nanoparticles produced from HNO_3 peptized sol–gels was achieved by using the nucleation–growth kinetic model described by Avrami–Erofe'ev.[53–55] This model is widely used for phase transitions and crystal growth processes in chemistry (eqn (3))

$$\alpha = 1-\exp[-(k(t - t_0))^m] \quad (3)$$

where α is the extent of reaction, k is the rate constant, t is the time coordinate, t_0 is the induction time and m is the Avrami exponent which depends on the reaction mechanism. The interpretation of m is based upon the work by Hulbert, who analyzed a series of possible ideal reactions and showed how the m values from the Avrami kinetic model can be correlated with a number of reaction mechanisms.[56] The values of m and k are most easily obtained using a Sharp–Hancock plot constructed by using eqn (4).[57]

$$\ln[-\ln(1 - \alpha)] = m\ln(t - t_0) + m\ln(k) \quad (4)$$

Thus a plot of $\ln[-\ln(1 - \alpha)]$ against $\ln(t - t_0)$ should yield a straight line with a gradient m and an intercept $m\ln(k)$, if the Avrami–Erofe'ev model is valid. The Sharp–Hancock plots based on the kinetic data derived from the (110) reflection peaks of TiO_2 (Fig. 2a–d) synthesized by *in situ* hydrothermal processes at 210, 230, 250 and 270 °C are shown in Fig. 2(e–h), respectively. The resultant plots exhibit a linear relationship within the range of $0.2 < \alpha < 0.8$, and the gradient (m) and intercepts ($m\ln(k)$) of lines have been determined by linear regression to compute the kinetic parameters (Table 1). The linear regression analysis gives an average error bar for each data point and the overall average error decreases as the reaction temperature increases from 210 °C to 270 °C.

It can be seen in Table 1 that the calculated values of m are 0.53, 0.44, 0.69 and 0.76 for the hydrothermal process of TiO_2 at 210, 230, 250 and 270 °C, respectively. Since the values of m are roughly within 0.5–1, it indicates that the hydrothermal reaction for the formation of rutile TiO_2 from the precursor gel occurs *via* a diffusion-controlled mechanism.[56] This means that the rate of diffusion of the reactants through the solution to the site of crystallization is the rate limiting factor of the overall reaction. The rates of all the other steps including breaking of the sol–gel structure upon heating to release the reactive species, formation of nuclei and crystal growth are relatively faster and therefore do not affect the overall rate of the reaction for the formation of TiO_2 nanoparticles under hydrothermal conditions.

It should be noted that the kinetic parameters k and m calculated from the Avrami–Erofe'ev kinetic model are reasonably consistent and within appropriate ranges, even though several factors may have influenced their accuracy during the experimental and data analysis stages. This includes, but not limited to, the complex nature of sol–gel used, EDXRD data collection over few visits to SRS station 16.4, possible variations in stirring speed of different cells used, detection of small diffraction peaks and errors in induction time due to the lower detection limits intrinsic to the EDXRD technique,[28] and errors in integration of the peak area which is a key parameter used for calculating the extent of reaction and other kinetic and mechanistic parameters. It is also worth mentioning here that the cooling process after the completion of the hydrothermal reactions can also be an important phenomenon. In this study, natural air cooling, which takes few hours, has been adapted for all the hydrothermal processes, but this cooling process was not monitored *in situ* due to limited availability of beamtime. The authors believe that natural air cooling has very little effect, if any, on crystal formation and growth processes. However, it would still be interesting to monitor *in situ* any changes during the cooling process of hydrothermal systems.

The products obtained from the *in situ* hydrothermal reactions carried out at Daresbury Laboratory have been further characterized by powder XRD and TEM to study the crystal structure, size and morphology. The XRD patterns of the oven dried powder samples, from *in situ* hydrothermal reactions carried out at Daresbury Laboratory at 210 °C, 230 °C and 270 °C, are shown in Fig. 3. This confirms that rutile phase TiO_2 has been produced from all the hydrothermal processes studied. The XRD peaks are indexed using the reference pattern JCPDS card 01-088-1172. There is no evidence of any other crystalline phase or impurity in any of the samples.

Table 1 Summary of the Avrami–Erofe'ev kinetic parameters for the hydrothermal synthesis of TiO_2 nanoparticles from HNO_3 peptized sol–gels at different temperatures

T (°C)	t_0 (s)	k (s^{-1})	m
210	2020	3.95×10^{-4}	0.53
230	1950	6.03×10^{-4}	0.44
250	1880	4.14×10^{-4}	0.69
270	1810	2.55×10^{-4}	0.76

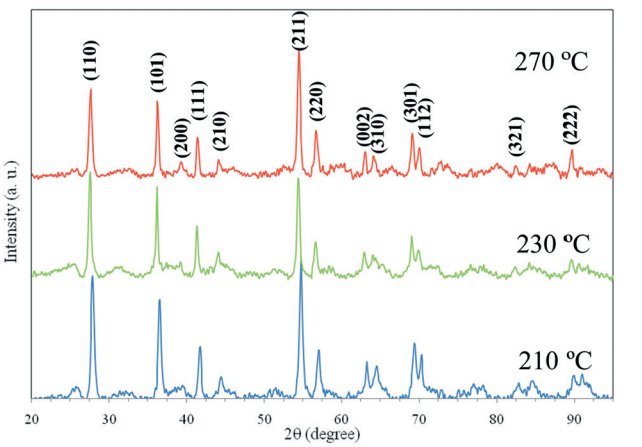

Fig. 3 XRD patterns of TiO_2 nanoparticles produced by *in situ* hydrothermal reactions of HNO_3 peptized sol–gels at 210 °C, 230 °C and 270 °C. Modified versions of our previously published XRD patterns.[50]

These powder XRD results are in good agreement with our *in situ* EDXRD results. The XRD pattern for the sample produced at 250 °C is missing because this sample was misplaced during laboratory shift and the repeat experiment was not possible due to unavailability of any further beamtime for this project. However, the authors have absolutely no doubt on this sample forming the same rutile phase TiO_2 particles because many *ex situ* hydrothermal synthesis experiments under similar process conditions have been conducted at the University of Leeds laboratories and the results are in complete agreement.

The TEM images of the TiO_2 nanoparticles produced by *in situ* hydrothermal reactions of HNO_3 peptized sol–gels at 210, 230, 250 and 270 °C are shown in Fig. 4a–d, respectively. It is evident from these images that the particles produced from all these processes generally exhibit bi-modal size and morphological features. The smaller spherical particles are found to be in the average size range of around 5–15 nm and the larger rod-like particles around 30–95 nm. The particles produced from the process at the highest temperature of 270 °C showed relatively narrower particle size and morphology distributions with fewer smaller spherical particles compared with the other processes studied at the lower temperatures.

The *in situ* EDXRD technology coupled with synchrotron radiation provides the capability to study reactions in very special conditions such as under very low or high temperatures and/or pressures, allowing very fast and time resolved measurements. This makes it possible to carry out detailed kinetic and mechanistic studies, which are not possible with conventional XRD. However, there are some limitations to this technology, for example it relies on the ability of the high energy beam of synchrotron radiation to penetrate through the steel walls of the pressure vessel. The thickness of the pressure vessel to be used, which controls the maximum safe working temperature and pressure conditions, depends on the maximum usable energy of synchrotron radiation, because the higher the X-ray energy the more penetrating the beam.[58] So far we have studied the hydrothermal reactions at a maximum temperature of 270 °C and pressure of 42 bar using a pressure vessel with a wall thickness of 0.25 mm at station 16.4 Daresbury Laboratory. However, different beamlines throughout the world have different levels of energies and capabilities that determine the maximum safe working temperature and pressure conditions at which one can study any hydrothermal system. Furthermore, *in situ* EDXRD is less sensitive due to high noise from the scattering background and has lower resolution than the conventional angular dispersive XRD. This is a general issue of *in situ* EDXRD techniques, which also makes particle sizing unfeasible.

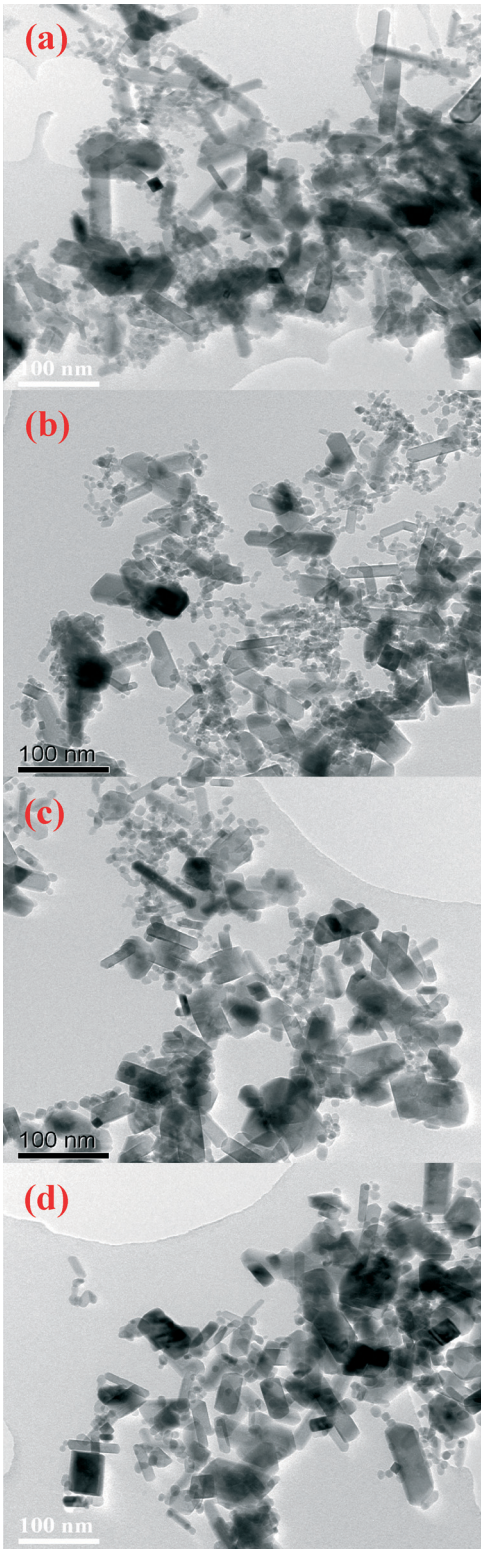

Fig. 4 TEM images of TiO_2 nanoparticles produced by *in situ* hydrothermal reactions of HNO_3 peptized sol–gels at (a) 210 °C, (b) 230 °C, (c) 250 °C and (d) 270 °C.

Conclusions

In situ EDXRD has been successfully used to study the evolution of crystalline TiO_2 nanoparticles from HNO_3 peptized sol–gels at 210, 230, 250 and 270 °C in the hydrothermal process. Pure rutile TiO_2 nanoparticles have been produced as confirmed by both *in situ* EDXRD and powder XRD data. The

reaction kinetics and mechanistic analysis of the hydrothermal synthesis of TiO_2 nanoparticles has been proposed based on the Avrami–Erofe'ev nucleation–growth kinetic model. It has been found that the hydrothermal synthesis of TiO_2 nanoparticles from the HNO_3 peptized sol–gel process exhibits a diffusion-controlled reaction mechanism. The TEM results have shown that the particles produced are below 100 nm in size and exhibit bi-modal particle size and morphology distribution. The fundamental understanding of reaction kinetics and the mechanism developed from these studies are very important for controlled synthesis of tailor-made nanoparticles employing the hydrothermal process.

Acknowledgements

The authors are thankful to EPSRC for funding the project, CCLRC for allowing access to SRS station 16.4 (Daresbury Laboratory, UK), IPSE and IMR (University of Leeds) for providing facilities and infrastructure to carry out this research investigation. The authors also thank D. J. Taylor and T. M. Bell, station scientists in station 16.4, for their assistance in setting up and running the synchrotron radiation experiments, and M. Ward for his assistance with the TEM analysis.

References

1 R. Wang, K. Hashimoto, A. Fujishima, M. Chikuni, E. Kojima, A. Kitamura, M. Shimohigoshi and T. Watanabe, *Nature*, 1997, **388**, 431.
2 N. O. Savage, S. A. Akbar and P. K. Dutta, *Sens. Actuators, B*, 2001, **72**, 239.
3 Y. Shimizu, N. Kuwano, T. Hyodo and M. Egashira, *Sens. Actuators, B*, 2002, **83**, 195.
4 B. O'Regan and M. Grätzel, *Nature*, 1991, **353**, 737.
5 K. Sunada, Y. Kikuchi, K. Hashimoto and A. Fujishima, *Environ. Sci. Technol.*, 1998, **32**, 726.
6 A. Fujishima, T. N. Rao and D. A. Tryk, *Electrochim. Acta*, 2000, **45**, 4683.
7 A. Fujishima, T. N. Rao and D. A. Tryk, *J. Photochem. Photobiol., C*, 2000, **1**, 1.
8 D. A. Tryk, A. Fujishima and K. Honda, *Electrochim. Acta*, 2000, **45**, 2363.
9 A. Hagfeldt and M. Graetzel, *Chem. Rev.*, 1995, **95**, 49.
10 A. L. Linsebigler, G. Lu and J. T. Y. Jr, *Chem. Rev.*, 1995, **95**, 735.
11 A. Millis and S. L. Hunte, *J. Photochem. Photobiol., A*, 1997, **108**, 1.
12 M. R. Hoffmann, S. T. Martin, W. Choi and D. W. Bahnemann, *Chem. Rev.*, 1995, **95**, 69.
13 M. A. Fox and M. T. Dulay, *Chem. Rev.*, 1993, **93**, 341.
14 X. Chen and S. S. Mao, *Chem. Rev.*, 2007, **107**, 2891.
15 Y. Oguri, R. E. Riman and H. K. Bowen, *J. Mater. Sci.*, 1998, **23**, 2897.
16 R. R. Bacsa and M. Grätzel, *J. Am. Ceram. Soc.*, 1996, **79**, 2185.
17 H. Cheng, J. Ma, Z. Zhao and L. Qi, *Chem. Mater.*, 1995, **7**, 663.
18 J. Yang, S. Mei and J. M. F. Ferreira, *J. Am. Ceram. Soc.*, 2000, **83**, 1361.
19 J. Yang, S. Mei and J. M. F. Ferreira, *J. Am. Ceram. Soc.*, 2001, **84**, 1696.
20 J. Yang, S. Mei and J. M. F. Ferreira, *J. Mater. Res.*, 2002, **17**, 2197.
21 J. Yang, S. Mei, J. M. F. Ferreira, P. Norby and S. Quaresma, *J. Colloid Interface Sci.*, 2005, **283**, 102.
22 K. Yanagisawa, Y. Yamamoto, Q. Feng and N. Yamasaki, *J. Mater. Res.*, 1998, **13**, 825.
23 H. Lee and G. M. Kale, *Int. J. Appl. Ceram. Technol.*, 2008, **5**, 657.
24 K. Byrappa and M. Yoshimura, *Handbook of Hydrothermal Technology*, ed. W. Andrew, Elsevier, Oxford and Waltham, 2nd edn, 2013, ch. 1, pp. 34–36.
25 A. J. Norquist and D. O'Hare, *J. Am. Chem. Soc.*, 2004, **126**, 6673.
26 A. K. Cheetham and C. F. Mellot, *Chem. Mater.*, 1997, **8**, 2269.
27 R. J. Francis and D. O'Hare, *J. Chem. Soc., Dalton Trans.*, 1998, 3133.
28 N. Yee, S. Shaw, L. G. Benning and T. H. Nguyen, *Am. Mineral.*, 2006, **91**, 92.
29 S. M. Clark, *Nucl. Instrum. Methods Phys. Res., Sect. A*, 1996, **381**, 161.
30 S. D. M. Jacques, K. Pile, P. Barnes, X. Lai, K. J. Roberts and R. A. Williams, *Cryst. Growth Des.*, 2005, **5**, 395.
31 R. J. Francis, S. J. Price, J. S. O. Evans, S. O'Brien and D. O'Hare, *Chem. Mater.*, 1996, **8**, 2102.
32 D. O'Hare, J. S. O. Evans, R. J. Francis, P. S. Halasyamani, P. Norby and J. Hanson, *Microporous Mesoporous Mater.*, 1998, **21**, 253.
33 F. Millange, R. I. Walton, N. Guillou, T. Loiseau, D. O'Hare and G. Ferey, *Chem. Mater.*, 2002, **14**, 4448.
34 S. Shaw, C. Michael, B. Henderson and S. M. Clark, *Am. Mineral.*, 2002, **87**, 533.
35 C. L. Cahill, L. G. Benning, H. L. Barnes and J. B. Parise, *Chem. Geol.*, 2000, **167**, 53.
36 J. S. O. Evans, S. J. Price, H. V. Wong and D. O'Hare, *J. Am. Chem. Soc.*, 1998, **120**, 10837.
37 A. M. Fogg, J. S. Dunn and D. O'Hare, *Chem. Mater.*, 1998, **10**, 356.
38 A. M. Fogg, J. S. Dunn, S. G. Shyu, D. R. Cary and D. O'Hare, *Chem. Mater.*, 1998, **10**, 351.
39 R. J. Francis, S. J. Price, S. Obrien, A. M. Fogg, D. O'Hare, T. Loiseau and G. Ferey, *Chem. Commun.*, 1997, 521.
40 S. Obrien, R. J. Francis, S. J. Price, D. O'Hare, S. M. Clark, N. Okazaki and K. Kuroda, *J. Chem. Soc., Chem. Commun.*, 1995, 2423.
41 K. A. Cheetham and F. M. Caroline, *Chem. Mater.*, 1997, **9**, 2269.
42 N. Blagden, R. Davey, M. Song, M. Quayle, S. Clark, D. Taylor and A. Nield, *Cryst. Growth Des.*, 2003, **3**, 197.
43 A. Jianu, L. Stanciu, J. R. Groza, C. Lathe and E. Burkel, *Nucl. Instrum. Methods Phys. Res., Sect. B*, 2003, **199**, 44.

44 L. B. Kirsch, E. K. Richman, A. E. Riley and S. H. Tolbert, *J. Phys. Chem. B*, 2004, **108**, 12698.
45 D. R. Hummer, J. D. Kubicki, P. R. C. Kent, J. E. Post and P. J. Heaney, *J. Phys. Chem. C*, 2009, **113**, 4240.
46 R. J. Francis and D. O'Hare, *J. Chem. Soc., Dalton Trans.*, 1998, 3133.
47 Y. Zhou, E. Antonova, W. Bensch and G. R. Patzke, *Nanoscale*, 2010, **2**, 2412.
48 Y. Zhou, E. Antonova, W. Bensch and G. R. Patzke, *Nanoscale*, 2010, **2**, 2412.
49 Y. Zhou, E. Antonova, Y. Lin, J. D. Grunwaldt, W. Bensch and G. R. Patzke, *Eur. J. Inorg. Chem.*, 2012, 783.
50 M. Rehan, X. Lai and G. M. Kale, *CrystEngComm*, 2011, **13**, 3725.
51 P. Barnes, A. C. Jupe, S. L. Colston, S. D. Jacques, A. Grant, T. Rathbone, M. Miller, S. M. Clark and R. J. Cernik, *Nucl. Instrum. Methods Phys. Res., Sect. B*, 1998, **134**, 310.
52 S. L. Colston, S. D. M. Jacques, P. Barnes, A. C. Jupe and C. Hall, *J. Synchrotron Radiat.*, 1998, **5**, 112.
53 M. Avrami, *J. Chem. Phys.*, 1939, **7**, 1103.
54 M. Avrami, *J. Chem. Phys.*, 1940, **8**, 212.
55 M. Avrami, *J. Chem. Phys.*, 1941, **9**, 177.
56 S. F. Hulbert, *J. Br. Ceram. Soc.*, 1969, **6**, 11.
57 J. D. Hancock and J. H. Sharp, *J. Am. Ceram. Soc.*, 1972, **55**, 74.
58 S. Shaw, C. M. B. Henderson, S. M. Clark, Y. Wang, *The Proceedings of Goldschmidt Conference*, Toulouse, France, 1998, pp. 1377.

